engineering proceedings

MDPI

Proceeding Paper

Ancient Projectile Identification Through Inverse Analysis Effects of Masonry Homogenization and Material Homogeneity †

Vincenzo Minutolo *, Eugenio Ruocco, Simone Palladino and Renato Zona *

Department of Engineering, Università della Campania Luigi Vanvitelli, Via Roma 29, 81031 Aversa, Italy; eugenio.ruocco@unicampania.it (E.R.); simone.palladino@unicampania.it (S.P.)

* Correspondence: vincenzo.minutolo@unicampania.it (V.M.); renato.zona@unicampania.it (R.Z.)

† Presented at the Discovering Pompeii II: From Digitally Surveyed Data to Visualized Simulations (SCORPiò-NIDI 2026), Aversa, Italy, 13 February 2026.

Abstract

The mechanical interpretation of impact traces on historical masonry structures offers a promising pathway for identifying the typology of ancient projectiles used in past conflicts. In recent years, inverse analysis approaches have been increasingly employed to infer projectile characteristics from residual damage patterns observed on archaeological remains. However, the reliability of such reconstructions strongly depends on the mechanical representation adopted for the impacted masonry. Ancient masonry walls, particularly those composed of tuff blocks and mortar joints, exhibit a marked heterogeneity that cannot always be adequately captured through simplified homogeneous material models. In this study, a numerical framework is developed to investigate how different assumptions regarding masonry homogenization influence the identification of projectile parameters derived from impact evidence. The mechanical response of the masonry is modeled through a homogenization procedure based on representative volume elements (RVE), allowing the heterogeneous brick—mortar assemblage to be translated into an equivalent macroscopic constitutive description. The resulting elastic and limit mechanical properties are then employed within a Finite Element Limit Analysis (FELA) formulation grounded in Melan's lower bound theorem to evaluate collapse mechanisms and energy dissipation during impact.The methodology is applied to a case study inspired by the masonry walls of Pompeii, where parametric variations in mortar thickness are considered to assess their influence on the homogenized stiffness and strength domain. The results highlight how even simplified yet mechanically consistent models are capable of capturing the anisotropic behavior of masonry and its implications for energy absorption. In particular, the study shows that adopting a homogenization-based representation leads to more reliable inverse estimates of projectile velocity and momentum compared to purely homogeneous approximations. Overall, the proposed approach provides a computationally efficient yet mechanically grounded framework for supporting archaeological interpretations of impact traces, contributing to a more quantitative understanding of ancient warfare technologies.

Keywords: limit analysis; Pompeian wall; ancient balista; masonry limit domain

Check for updates

Academic Editor: Giovanni Loreto

Published: 12 August 2026

Copyright: © 2026 by the authors. Licensee MDPI, Basel, Switzerland. This article is an open access article distributed under the terms and conditions of the Creative Commons Attribution (CC BY) license.

1. Introduction

The identification of ancient war projectiles through the mechanical interpretation of residual impact traces on masonry structures represents a multidisciplinary research field at the intersection of structural mechanics, fracture mechanics, material science, archeology,

and computational modeling. Inverse analysis techniques have progressively emerged as powerful tools for reconstructing projectile characteristics—such as velocity, momentum, and impact energy—from measurable geometric damage patterns on historical structures.

The northern walls of Pompeii constitute a paradigmatic case study. Detailed geometric surveys of anthropic cavities and impact craters have been conducted using advanced measurement and visualization techniques, allowing quantitative characterization of crater morphology and spatial distribution [1–3]. These investigations provide a robust geometric foundation for mechanical back-analysis aimed at distinguishing ballistic impacts from natural degradation phenomena.

A critical issue in inverse ballistic assessments concerns the mechanical representation of masonry. Ancient tuff masonry exhibits strong heterogeneity due to porosity, block arrangement, mortar interfaces, weathering, and micro-cracking. Consequently, the assumption of material homogeneity may significantly influence the evaluation of collapse mechanisms and energy dissipation.

Homogenization techniques bridge mesoscopic heterogeneity and macroscopic constitutive modeling. Early bounds for effective elastic properties were proposed by Voigt [4] and Reuss [5], later unified through the Hill average [6]. Variational bounds for composite materials were further refined by Hashin and Shtrikman [7]. Mean-field approaches such as Mori–Tanaka schemes [8] and representative volume element (RVE) frameworks [9] allow the derivation of equivalent continuum properties for heterogeneous media.

In masonry modeling, homogenization approaches have been extensively applied to periodic block structures and stone assemblages [10,11]. Multi-scale strategies enable the evaluation of equivalent stiffness, strength, and fracture energy parameters consistent with the underlying mesostructure.

Fracture mechanics provides an essential theoretical framework for evaluating energy dissipation during impact. Griffith's energy balance criterion [12] and Irwin's stress intensity factor formulation [13] establish the relationship between crack propagation and energy release rate. In heterogeneous and graded materials, fracture parameters are strongly affected by spatial property variation, as demonstrated in functionally graded plate analyses [14].

Plastic collapse and limit analysis formulations further contribute to energy-based interpretations of impact damage. Semi-analytical limit analysis of masonry domes [15] and dislocation-based finite element procedures for plastic collapse assessment [16] highlight the sensitivity of collapse multipliers to material modeling assumptions. From a geomechanical perspective, local collapse phenomena in weak rocks are governed by combined shear failure and tensile cracking mechanisms analogous to impact-induced crater formation in tuff masonry [17,18].

Recent studies on dynamic fracture of rock-like materials [19,20] confirm that energy dissipation mechanisms in geomaterials are strongly influenced by porosity and microstructural heterogeneity. Therefore, adopting a mechanically consistent homogenized model is essential to avoid systematic overestimation or underestimation of projectile kinetic energy in inverse analyses.

In inverse ballistic modeling, two alternative strategies may be adopted: (i) global homogeneous equivalent modeling, where impact effects are evaluated through equivalent static loading and energy balance principles; (ii) mechanically informed homogenization calibrated through fracture energy and plastic dissipation parameters derived from mesoscale considerations. The choice between these strategies directly affects reconstructed projectile velocity and momentum.

The present work investigates how different masonry homogenization assumptions influence the inverse identification of ancient projectiles. By comparing homogeneous

equivalent models with advanced homogenized descriptions, the study quantifies the sensitivity of reconstructed ballistic parameters to material modeling choices. The objective is to provide a mechanically rigorous framework for ancient projectile identification, highlighting the central role of homogenization theory in inverse analysis procedures applied to historical masonry structures.

2. Materials and Methods

This section presents the theoretical framework adopted for the numerical modeling of elasto-plastic materials under small strain assumptions. The formulation follows a strain-driven continuum mechanics approach based on the standard additive decomposition of the infinitesimal strain tensor into elastic and plastic components. The elastic behavior is derived from a strain energy density function, while the inelastic response is governed by a yield criterion combined with an associated flow rule.

The governing equilibrium equations are formulated in both strong and weak forms, enabling their discretization within the finite element method. A formulation specifically suited for limit analysis is introduced through a Finite Element Limit Analysis (FELA) framework. In this setting, the stress field is decomposed into an elastic contribution and a self-equilibrated component, in accordance with Melan's lower bound theorem.

Finally, a homogenization procedure is employed to link microstructural fields to effective macroscopic material parameters through volume averaging over a representative volume element (RVE). The proposed framework provides a consistent basis for investigating failure mechanisms in heterogeneous media and for evaluating their macroscopic response under complex loading conditions.

2.1. Finite Element Discretization and Limit Load Analysis

The displacement-based finite element method assumes the existence of a kinematically admissible displacement field over the domain. The structure is discretized into elements interconnected at nodes, where the displacement field is interpolated using shape functions and nodal displacement values. Compatibility is enforced at the nodal level, ensuring continuity of the displacement field across element boundaries.

By enforcing equilibrium in weak form and assembling elemental contributions, the global equilibrium equation can be expressed as

$$\mathbf{F} = \mathbf{K}\mathbf{u} \tag{1}$$

where $\mathbf{u}$ is the vector of nodal displacements, $\mathbf{F}$ the vector of external nodal forces, and $\mathbf{K}$ the global stiffness matrix.

Inelastic behavior is traditionally incorporated by allowing permanent strains to develop once the stress state reaches the yield surface. The evolution of plastic strains is governed by the normality rule, and incremental return-mapping algorithms are typically used for numerical implementation.

In the present work, an alternative strategy based on the lower bound theorem of limit analysis is adopted. The collapse load is computed directly by searching for admissible self-equilibrated stress fields. These stresses give rise to equivalent nodal forces, which depend linearly on displacement-like parameters $\mathbf{v}^p$ through an operator $\mathbf{H}$.

Applying the Bubnov–Galerkin procedure to the weak form of equilibrium yields

$$\mathbf{F} = \mathbf{K}\mathbf{u} - \mathbf{H}\mathbf{v}^p \tag{2}$$

where $\mathbf{H}$ collects the contributions of self-equilibrated stresses at the element level. The vector $\mathbf{v}^p$ represents nodal dislocation-like parameters associated with residual stress fields.

https://doi.org/10.3390/engproc2026149007

The problem can therefore be decomposed into elastic and self-equilibrated components:

$$\begin{aligned} \mathbf{F} &= \mathbf{K}\mathbf{u}^{e} \\ \mathbf{K}\mathbf{u}^{0} - \mathbf{H}\mathbf{v}^{p} &= \mathbf{0} \end{aligned} \tag{3}$$

where $\mathbf{u}^{e}$ denotes the elastic displacement field and $\mathbf{u}^{0}$ the self-equilibrated displacement field.

The associated self-equilibrated stress field can be expressed as

$$\sigma^{0} = \boldsymbol{\mathcal{V}}\,\delta(\mathbf{v}^{p}, \mathbf{u}^{0}) \tag{4}$$

where $\boldsymbol{\mathcal{V}}$ is the operator mapping displacement discontinuities to stress space, and δ represents the superimposed element-wise displacement field satisfying compatibility constraints.

Melan's Theorem

According to Bleich [21] and Melan [22]:

> A structure subjected to a time-dependent load $f(t)$ does not collapse if and only if there exists a time-independent self-equilibrated stress field $\bar{\sigma}_0$ such that the sum of this field and the elastic stress $\sigma_e(t)$ remains admissible at all times.

This principle can be reformulated as the following optimization problem:

$$k^{*} = \sup_{\delta}\left\{ k \;\middle|\; f\left(k\,\sigma^{e}(\mathbf{u}^{e}) + \sigma^{0}(\delta)\right) \leq 0 \right\} \tag{5}$$

where k^{*} represents the collapse multiplier and $f(\cdot)$ denotes the yield function, and we recognize, through Equation (4), that the set of the self-equilibrated stress is defined in the domain spanned by δ.

2.2. Homogenization

To connect microstructural behavior with macroscopic material response, volume averaging over a representative volume element (RVE) is adopted. The macroscopic strain and stress tensors are defined as

$$\begin{aligned} \langle \boldsymbol{\varepsilon} \rangle &= \frac{1}{|V|} \int_{V_{RVE}} \boldsymbol{\varepsilon}(\mathbf{x})\, \mathrm{d}V \\ \langle \boldsymbol{\sigma} \rangle &= \frac{1}{|V|} \int_{V_{RVE}} \boldsymbol{\sigma}(\mathbf{x})\, \mathrm{d}V \end{aligned} \tag{6}$$

where $|V|$ denotes the RVE volume, and $\boldsymbol{\varepsilon}(\mathbf{x})$, $\boldsymbol{\sigma}(\mathbf{x})$ are the local strain and stress fields.

Assuming isotropic linear elastic macroscopic behavior, the effective material parameters $\boldsymbol{\kappa}$ are identified by minimizing the discrepancy between averaged microstructural stresses and macroscopic constitutive predictions:

$$\boldsymbol{\kappa}^{*} = \arg\min_{\boldsymbol{\kappa}} \sum_{i=1}^{N} \left\| \langle \boldsymbol{\sigma}_i \rangle - \frac{\partial w(\langle \boldsymbol{\varepsilon}_i \rangle)}{\partial \boldsymbol{\varepsilon}} \right\|_{2/F} \tag{7}$$

where w is the strain energy density function, N is the number of loading cases, and $\|\cdot\|_{2/F}$ denotes either the Euclidean norm or the Frobenius norm, depending on the adopted stress representation.

https://doi.org/10.3390/engproc2026149007

2.3. Constitutive Equations

In this work, the constitutive response is described by a *convex* elastic domain D_e in stress space. Admissible stresses belong to the closure $\overline{D}_e = \mathring{D}_e \cup \partial D_e$, where $\mathring{D}_e$ and ∂D_e denote the interior and the boundary of the domain, respectively; stress states outside $\overline{D}_e$ are not admissible. The set D_e contains the origin, so that the null stress state (corresponding to null external actions) is always feasible.

For stress paths entirely contained in $\mathring{D}_e$, the response is reversible and therefore purely elastic. Plastic (permanent) strain rates $\dot{\boldsymbol{\varepsilon}}^p$ develop when the stress reaches the yield surface ∂D_e and, under continued loading, the stress remains on ∂D_e. The plastic flow is assumed associated (normality rule),

$$\dot{\boldsymbol{\varepsilon}}^p = \dot{\lambda}\, \mathbf{n}(\partial D_e), \tag{8}$$

where $\mathbf{n}$ is the outward unit normal to ∂D_e (defined almost everywhere) and $\dot{\lambda} \geq 0$ is the plastic multiplier. This assumption is consistent with the stability postulate

$$\mathrm{d}\boldsymbol{\sigma} : \dot{\boldsymbol{\varepsilon}}^p \geq 0, \tag{9}$$

which provides a classical sufficient condition for dissipativity in rate-independent plasticity [23].

When plastic strains are present, the elastic law is written in terms of the elastic strain $\boldsymbol{\varepsilon}^e = \boldsymbol{\varepsilon}^* - \boldsymbol{\varepsilon}^p$, leading to

$$\boldsymbol{\sigma} = \mathcal{C}(\boldsymbol{\varepsilon}^* - \boldsymbol{\varepsilon}^p), \tag{10}$$

where $\mathcal{C}$ is the symmetric fourth-order elasticity tensor.

The admissible domain is defined through a yield function $f(\boldsymbol{\sigma})$ as

$$D_e = \left\{ \boldsymbol{\sigma} = \{\sigma_x, \sigma_y, \sigma_z, \tau_{xy}, \tau_{xz}, \tau_{yz}\} \;\middle|\; f(\boldsymbol{\sigma}) \leq 0 \right\}. \tag{11}$$

Comprehensive overviews of constitutive modeling, yield surfaces, and internal-variable formulations (hardening/softening and, more generally, inelastic evolution laws) can be found in standard references [24,25]. In many engineering materials, the elastic domain boundary can be represented by smooth algebraic surfaces, frequently quadratic, possibly evolving in stress space due to internal variables [26,27].

For isotropic materials, the elastic domain is invariant with respect to material rotations and can be expressed in terms of principal stresses σ_ξ, σ_η, σ_ζ. For anisotropic materials, D_e depends on both the stress components and the material symmetry directions; a classical formulation for anisotropic yielding and plastic flow is due to Hill [28]. Consequently, the domain is generally expressed in the material principal frame through the six stress components $\sigma_x, \sigma_y, \sigma_z, \tau_{xy}, \tau_{xz}, \tau_{yz}$.

For ductile metals, the von Mises criterion implies insensitivity to hydrostatic stress; the yield surface is cylindrical around the hydrostatic axis $\sigma_\xi = \sigma_\eta = \sigma_\zeta$ (in the Haig-Westergaard space). In contrast, quasi-brittle and frictional materials (including masonry and tuff-like geomaterials) exhibit strength asymmetry in tension/compression and pronounced directional effects, which motivate anisotropic and "aniso-resistant" domains. In masonry mechanics, such choices are often coupled with no-tension or unilateral assumptions and limit analysis concepts [29–31].

In the present study, a translated quadratic criterion is adopted to account simultaneously for anisotropy and different tensile/compressive strengths. This choice can be interpreted as a modified Hill-type surface, consistent with the Tsai–Wu family of crite-

ria [27]. Similar formulations have been used in the literature for orthotropic media and masonry-like strength domains [32,33]. In plane stress, the yield function reads

$$f(\sigma) = 1 - \left(\frac{1}{s_{xc}} + \frac{1}{s_{xt}}\right)\sigma_x - \left(\frac{1}{s_{yc}} + \frac{1}{s_{yt}}\right)\sigma_y - \frac{\sigma_x^2}{s_{xc}s_{xt}} - \frac{\sigma_y^2}{s_{yc}s_{yt}} - \frac{\tau_{xy}^2}{s_{xy}^2}, \tag{12}$$

where $s_{\alpha t}$ and $s_{\alpha c}$ ($\alpha \in \{x, y\}$) denote the tensile and compressive strengths along the material directions, and $s_{xy} = s_{xyt} = -s_{xyc}$ is the shear strength.

A typical anisotropic limit locus is shown in Figure 1. The adopted strength description is later combined with the lower-bound limit analysis setting used in this work to determine collapse multipliers and admissible self-equilibrated stress fields [15,16,22,34].

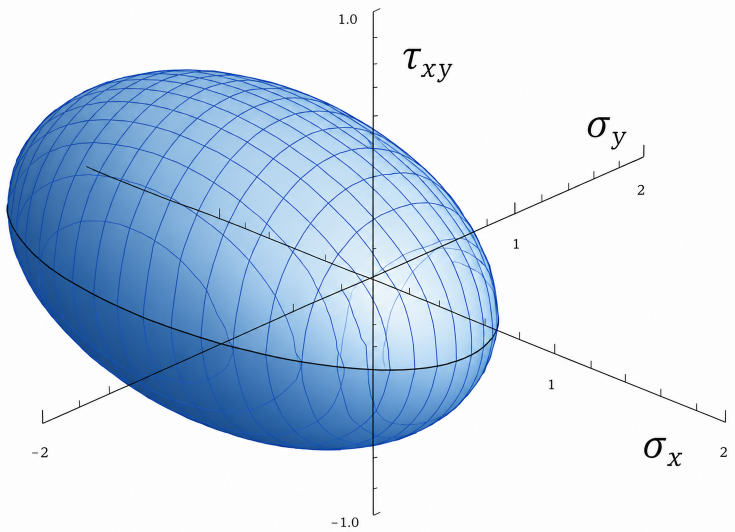


Figure 1. Anisotropic limit domain: $-1 \leq \sigma_x \leq 0.5 = -2, -2 \leq \sigma_y \leq 0.75, -0.6 \leq \tau_{xy} \leq 0.6$.

3. Case Study: Pompeian Masonry Wall

The case study concerns the mechanical characterization of a Pompeian masonry wall through a homogenization-based approach. The first step of the analysis consisted in identifying a Representative Volume Element (RVE) of the masonry texture, as shown in Figure 2.

In the context of masonry, an RVE is defined as the smallest portion of material that statistically represents the periodic arrangement of bricks and mortar joints, such that the volume-averaged stress and strain fields coincide with the macroscopic response of the wall. For running-bond masonry, the RVE must include both horizontal and vertical mortar interfaces in order to properly capture anisotropy induced by the brick—mortar pattern. The effective elastic and limit properties of the masonry RVE were derived through the application of fundamental stress states, as schematically illustrated in Figure 3. In particular, independent macroscopic loading conditions were imposed corresponding to uniaxial tension/compression along the horizontal direction (σ_x), uniaxial tension/compression along the vertical direction (σ_y), and in-plane shear (τ_{xy}).

For the elastic characterization, each loading case was applied within the linear regime, and the homogenized stress–strain response was obtained through volume averaging of the microstructural fields. The effective elastic moduli E_{xx} and E_{yy}, together with the Poisson ratios ν_{xy} and ν_{yx}, were computed from the slope of the macroscopic stress-strain curves under the corresponding fundamental deformation modes. For the limit (plastic) characterization, the same set of fundamental loadings was considered within the FELA

framework. The collapse multiplier associated with each stress state was determined according to the lower-bound theorem, providing the homogenized limit stresses in tension, compression, and shear. In this manner, both the elastic stiffness tensor and the effective strength domain of the masonry were consistently identified from the response of the RVE to elementary stress states. This procedure ensures that the macroscopic constitutive parameters—both elastic and plastic—are directly rooted in the mechanical behavior of the heterogeneous brick—mortar assembly, preserving the anisotropy induced by the masonry pattern.

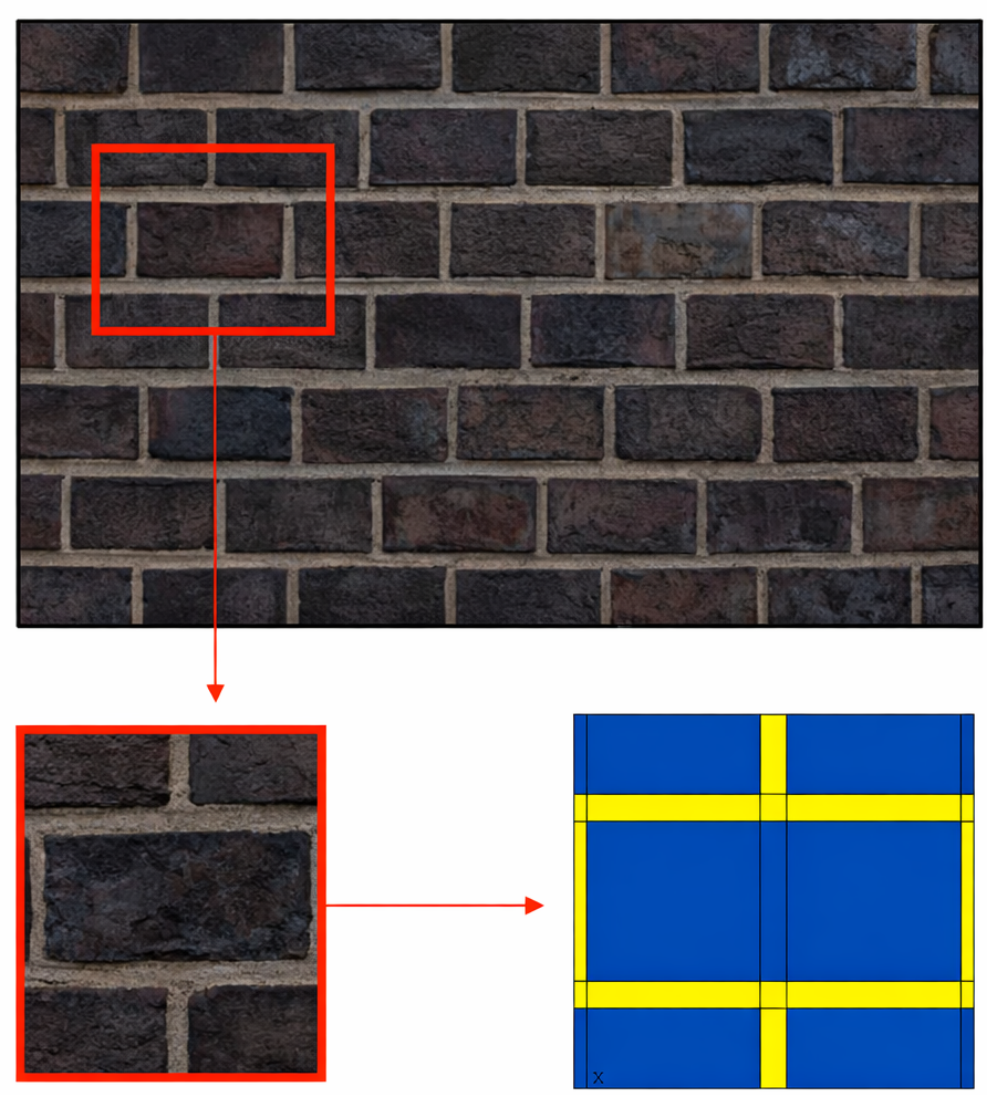


Figure 2. Extraction and idealization of the Representative Volume Element (RVE) from the Pompeian masonry wall. (**Top**): real masonry texture with highlighted RVE region. (**Bottom left**): zoomed portion of the selected masonry pattern. (**Bottom right**): geometrical idealization of the RVE used for homogenization, where bricks are represented in blue and mortar joints in yellow.

Four different configurations were considered by varying the mortar inclusion thickness t, corresponding to different mortar–brick ratios: $t = 5$ mm (case a), $t = 10$ mm (case b), $t = 15$ mm (case c), and $t = 25$ mm (case d). In Figure 2 is represented the extraction of the RVE from the wall. This parametric variation allows evaluation of the influence of mortar content on the effective mechanical response.

Elastic homogenization was first performed using Voigt and Reuss bounds. The constituent elastic properties were assumed as $E_{\text{brick}} = 3800$ MPa, $\nu_{\text{brick}} = 0.2$, and $E_{\text{mortar}} = 1000$ MPa, $\nu_{\text{mortar}} = 0.25$. The resulting homogenized orthotropic elastic parameters

$(E_{xx}, E_{yy}, \nu_{xy}, \nu_{yx})$ were evaluated for each mortar thickness. As expected, increasing mortar content leads to a progressive reduction in effective stiffness, with more pronounced anisotropic effects for larger joint thicknesses. The considered load cases is reported in Figure 3. The discretization of the RVE is reported in Figure 4. The results are reported in the following Tables 1 and 2.

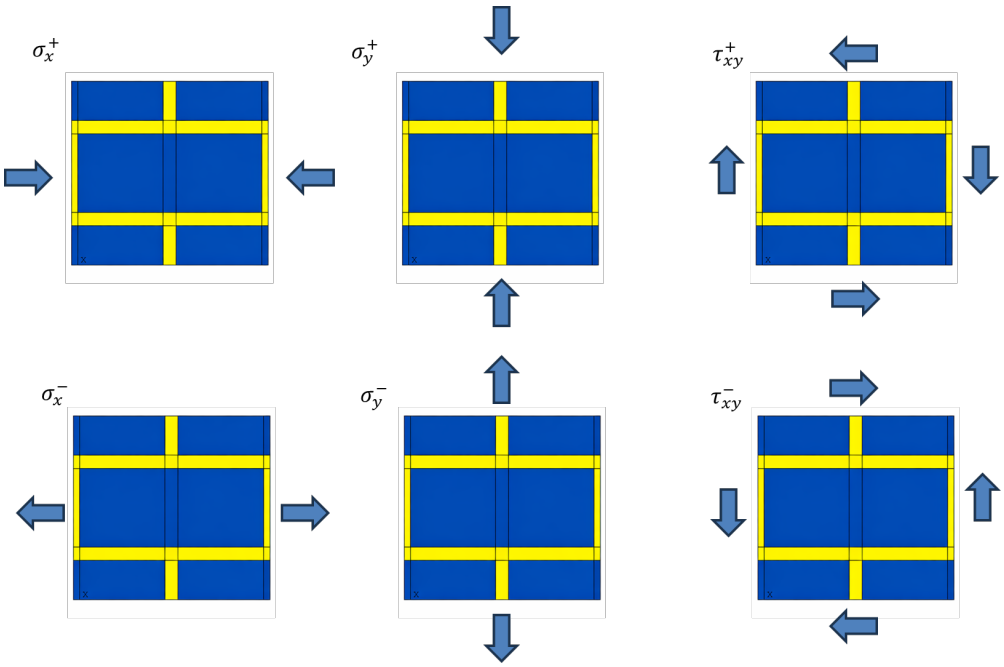


Figure 3. Fundamental macroscopic stress states applied to the masonry Representative Volume Element (RVE) for homogenization purposes. (**Top row**): positive loading directions corresponding to uniaxial stress in the horizontal direction (σ_x), uniaxial stress in the vertical direction (σ_y), and in-plane shear stress (τ_{xy}). (**Bottom row**): reversed loading directions used to ensure consistency of the homogenized elastic and limit responses. The RVE distinguishes brick phase (blue) and mortar joints (yellow).

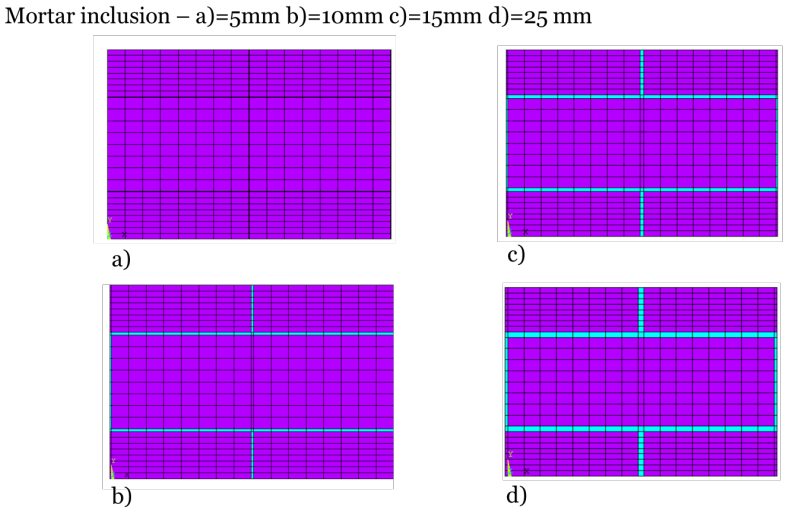


Figure 4. Parametric variation of the Representative Volume Element (RVE) adopted for the Pompeian masonry wall. Four configurations are shown corresponding to increasing mortar inclusion thickness ($t = 5$ mm, 10 mm, 15 mm, 25 mm). The brick phase and mortar joints are explicitly represented in the geometrical model, allowing evaluation of the influence of the mortar–brick ratio on the homogenized elastic and limit mechanical properties.

Table 1. Elastic homogenized properties of the masonry RVE obtained using the Reuss bound.

RVE	t [mm]	E_{xx}^{-} [MPa]	E_{yy}^{-} [MPa]	ν_{xy}^{-}	ν_{yx}^{-}
a	5	3756.9	3671.5	0.2008	0.1962
b	10	3714.7	3551.4	0.2015	0.1927
c	15	3673.5	3438.9	0.2023	0.1893
d	25	3593.8	3234.0	0.2037	0.1833

Table 2. Elastic homogenized properties of the masonry RVE obtained using the Voigt bound.

RVE	t [mm]	E_{xx}^{+} [MPa]	E_{yy}^{+} [MPa]	ν_{xy}^{+}	ν_{yx}^{+}
a	5	3788.5	3765.0	0.2002	0.1990
b	10	3777.0	3730.0	0.2004	0.1979
c	15	3765.6	3695.0	0.2006	0.1969
d	25	3742.6	3625.0	0.2010	0.1947

Subsequently, plastic (limit) homogenization was carried out within the FELA framework [35].

Limit stresses were assigned separately to brick and mortar constituents and the corresponding homogenized strength domain was determined through lower-bound limit analysis. The limit stresses considered for the constituents and the resulting homogenized RVE strengths are reported in Table 3. The effective tensile and compressive strengths along the principal material directions, as well as the shear strength τ_{xy}, were found to be strongly influenced by the mortar–brick ratio. In particular, the increase of mortar thickness reduces the homogenized compressive and shear capacities, while modifying the anisotropic shape of the yield surface. This combined elastic and plastic homogenization procedure provides the effective macroscopic parameters required for subsequent inverse analysis of projectile impact, ensuring that both stiffness and strength characteristics of the heterogeneous masonry are consistently represented.

Table 3. Limit stresses of brick, mortar and homogenized RVE obtained through FELA-based plastic homogenization.

Stress Component	Brick [MPa]	Mortar [MPa]	Homogenized RVE [MPa]
σ_x^{+}	2	0.25	0.47
σ_x^{-}	20	3	5.61
σ_y^{+}	2	0.25	3.42
σ_y^{-}	20	3	0.35
τ_{xy}	5	0.30	0.51

4. Discussion and Conclusions

The results obtained from the elastic and plastic homogenization analyses highlight the strong influence of the mortar–brick ratio on the effective mechanical response of the Pompeian masonry wall. Even though the adopted RVE geometry represents a simplified idealization of the real masonry texture, the model preserves the essential morphological features of the brick-–mortar arrangement, including orthotropic stiffness and directional strength asymmetry.

The elastic homogenization performed through Voigt and Reuss bounds shows a systematic reduction of the effective Young's moduli with increasing mortar thickness. Moreover, a clear anisotropic behavior emerges, as evidenced by the differences between E_{xx} and E_{yy} and between ν_{xy} and ν_{yx}. These differences are not artifacts of the numerical scheme but arise directly from the geometric configuration of horizontal and vertical joints.

https://doi.org/10.3390/engproc2026149007

Therefore, even within a simplified RVE framework, the masonry cannot be treated as isotropic without introducing non-negligible errors in the global stiffness description.

The plastic homogenization carried out within the FELA framework further emphasizes the directional dependence of the strength domain. The homogenized limit stresses differ significantly between tension and compression and between the two principal directions. This asymmetry reflects both the intrinsic mechanical contrast between brick and mortar and the structural role of the mortar joints in governing failure mechanisms. The resulting yield surface of the RVE is markedly anisotropic and non-symmetric, which is consistent with the mechanical behavior expected for historical masonry.

From the perspective of inverse analysis, these findings are particularly relevant. The identification of ancient projectile characteristics from impact craters relies critically on an accurate estimation of the energy dissipation capacity and collapse load of the wall material. If the masonry were modeled as a homogeneous isotropic medium with averaged properties, the predicted collapse multipliers and energy absorption would be distorted, leading to potentially misleading estimates of projectile velocity and momentum.

By contrast, the proposed homogenization-based approach provides an effective macroscopic constitutive model that is both computationally efficient and mechanically consistent with the heterogeneous microstructure. The RVE-based formulation allows the inverse engineering procedure to account for anisotropy, tension–compression asymmetry, and shear strength reduction, all of which directly affect impact-induced cracking and plastic dissipation.

In conclusion, the numerical modeling strategy adopted in this study demonstrates that a simplified yet mechanically realistic representation of the masonry wall significantly improves the reliability of inverse ballistic analyses. The combination of geometric idealization, elastic homogenization, and FELA-based limit characterization offers a robust framework for reconstructing projectile typology from residual impact evidence. In particular, the derived homogenized limit domain can be used to evaluate plastic dissipation at the projectile impact and perform the energy balance, as already described in a previous paper on the same argument for isotropic masonry models [36]. Such an approach strengthens the mechanical credibility of archaeological interpretations and enhances the quantitative assessment of ancient warfare technologies.

Author Contributions: Conceptualization, V.M. and R.Z.; methodology, V.M.; software, V.M. and R.Z.; validation, V.M. and E.R.; formal analysis, R.Z. and S.P.; investigation, R.Z. and S.P.; resources, V.M.; data curation, R.Z. and E.R.; writing—original draft preparation, V.M. and R.Z.; writing—review and editing, V.M., R.Z., E.R. and S.P.; visualization, R.Z.; supervision, V.M. and E.R.; project administration, V.M.; funding acquisition, V.M. All authors have read and agreed to the published version of the manuscript.

Funding: This research received no external funding.

Institutional Review Board Statement: Not applicable.

Informed Consent Statement: Not applicable.

Data Availability Statement: The original contributions presented in this study are included in the article.

Conflicts of Interest: The authors declare no conflicts of interest.

Abbreviations

The following abbreviations are used in this manuscript:

FELA	Finite Element Limit Analysis
RVE	Representative Volume Element

References

1. Bertacchi, S.; Gonizzi Barsanti, S.; Rossi, A. Geometry of Wall Degradation: Measuring and Visualising Impact Craters in the Northern Walls of Pompeii. *SCIRES-IT Sci. Res. Inf. Technol.* **2024**, *14*, 111–128.
2. Rossi, A.; Bertacchi, S.; Formicola, C.; Gonizzi Barsanti, S. Small anthropogenic indentations found in the unearthed city walls of Cornelia Veneria Pompeii (Piccole indentazioni antropiche rinvenute nella riesumata cinta urbica di Cornelia Veneria Pompeii). *Disegn. IDEE Immagin.* **2025**, *69*, 54–67. (In Italian)
3. Rossi, A.; Gonizzi Barsanti, S.; Bertacchi, S. Natural or anthropic? Measurement and visualisation of wall cavities in city walls. In *Transitions*; Franco Angeli: Milano, France, 2024.
4. Voigt, W. Ueber die Beziehung zwischen den beiden Elasticitätsconstanten isotroper Körper. *Ann. Phys.* **1889**, *274*, 573–587. [CrossRef]
5. Reuss, A. Berechnung der Fließgrenze von Mischkristallen. *Z. Angew. Math. Mech.* **1929**, *9*, 49–58. [CrossRef]
6. Hill, R. The Elastic Behaviour of a Crystalline Aggregate. *Proc. Phys. Soc. A* **1952**, *65*, 349–354. [CrossRef]
7. Hashin, Z.; Shtrikman, S. A Variational Approach to the Theory of the Elastic Behaviour of Multiphase Materials. *J. Mech. Phys. Solids* **1963**, *11*, 127–140. [CrossRef]
8. Mori, T.; Tanaka, K. Average Stress in Matrix and Average Elastic Energy of Materials with Misfitting Inclusions. *Acta Metall.* **1973**, *21*, 571–574. [CrossRef]
9. Kanit, T.; Forest, S.; Galliet, I.; Mounoury, V.; Jeulin, D. Determination of the Size of the Representative Volume Element for Random Composites. *Int. J. Solids Struct.* **2003**, *40*, 3647–3679. [CrossRef]
10. Luciano, R.; Sacco, E. Homogenization Technique and Damage Model for Masonry Material. *Int. J. Solids Struct.* **1997**, *34*, 3191–3208. [CrossRef]
11. Lourenço, P.B. Experimental and Numerical Issues in the Modelling of the Mechanical Behaviour of Masonry. *Constr. Build. Mater.* **1998**, *12*, 317–326.
12. Griffith, A.A. The Phenomena of Rupture and Flow in Solids. *Philos. Trans. R. Soc. A* **1921**, *221*, 163–198. [CrossRef]
13. Irwin, G.R. Analysis of Stresses and Strains Near the End of a Crack Traversing a Plate. *J. Appl. Mech.* **1957**, *24*, 361–364. [CrossRef]
14. Palladino, S.; Esposito, L.; Ferla, P.; Zona, R.; Minutolo, V. Functionally Graded Plate Fracture Analysis Using the Field Boundary Element Method. *Appl. Sci.* **2021**, *11*, 8465. [CrossRef]
15. Zona, R.; Ferla, P.; Minutolo, V. Limit Analysis of Conical and Parabolic Domes Based on Semi-Analytical Solution. *J. Build. Eng.* **2021**, *44*, 103271. [CrossRef]
16. Zona, R.; Minutolo, V. A Dislocation-Based Finite Element Method for Plastic Collapse Assessment in Solid Mechanics. *Arch. Appl. Mech.* **2024**, *94*, 1531–1552. [CrossRef]
17. Minutolo, V.; Gesualdo, A.; Nunziante, L. Local Collapse in Soft Rock Bank Cavities. *J. Geotech. Geoenviron. Eng.* **2001**, *127*, 1037–1042. [CrossRef]
18. Heap, M.J.; Violay, M.E. The Mechanical Behaviour and Failure Modes of Volcanic Rocks. *Bull. Volcanol.* **2021**, *83*, 33. [CrossRef]
19. Liu, K.; Zhao, J. Progressive Damage Behaviours of Triaxially Confined Rocks Under Multiple Dynamic Loads. *Rock Mech. Rock Eng.* **2021**, *54*, 573–590. [CrossRef]
20. Pei, G.; Xiao, D.; Zhang, M.; Jiang, J.; Xie, J.; Li, X.; Guo, J. Dynamic Fracture Properties of Defective Basalt Fiber Concrete Materials. *Materials* **2024**, *17*, 6275. [CrossRef] [PubMed]
21. Bleich, H.H. Über die Bemessung statisch unbestimmter Stahltragwerke unter Berücksichtigung des elastisch-plastischen Verhaltens des Baustoffes. *Bauingenieur* **1932**, *13*, 261–267.
22. Melan, E. Der Spannungszustand eines Mises-Hencky'schen Kontinuums bei veränderlicher Belastung. *Sitzungsber. Akad. Wiss. Wien Math.-Naturwiss. Kl. Abt. IIa* **1938**, *147*, 73–87.
23. Hill, R. *The Mathematical Theory of Plasticity*; Oxford University Press: New York, NY, USA, 1998; p. 366.
24. Lemaitre, J. *Handbook of Materials Behavior Models, Three-Volume Set: Nonlinear Models and Properties*; Academic Press: New York, NY, USA, 2001.
25. Lubliner, J. *Plasticity Theory*; Macmillan Co.: New York, NY, USA, 1990.
26. Wu, E.M. Phenomenological Anisotropic Failure Criterion. In *Mechanics of Composite Materials: Composite Materials*; Sendeckyj, G.P., Ed.; Academic Press Inc.: New York, NY, USA, 1974; Volume 2, pp. 353–431.
27. Tsai, S.W.; Wu, E.M. A General Theory of Strength for Anisotropic Materials. *J. Compos. Mater.* **1971**, *5*, 58–80. [CrossRef]
28. Hill, R. A Theory of the Yielding and Plastic Flow of Anisotropic Metals. *Proc. R. Soc. Lond. A* **1948**, *193*, 281–297. [CrossRef]
29. Heyman, J. The Stone Skeleton. *Int. J. Solids Struct.* **1966**, *2*, 249–279. [CrossRef]
30. Del Piero, G. Limit Analysis and No-Tension Materials. *Int. J. Plast.* **1998**, *14*, 259–271. [CrossRef]
31. Bruggi, M.; Taliercio, A. Analysis of No-Tension Structures Under Monotonic Loading Through an Energy-Based Method. *Comput. Struct.* **2015**, *159*, 1–12. [CrossRef]
32. Bruggi, M.; Taliercio, A. Topology Optimization of the Fiber-Reinforcement Retrofitting Existing Structures. *Int. J. Solids Struct.* **2013**, *50*, 121–136. [CrossRef]

33. Bertani, G.; Patruno, L.; D'Altri, A.M.; Castellazzi, G.; de Miranda, S. A Single-Surface Multi-Failure Strength Domain for Masonry. *Int. J. Solids Struct.* **2024**, *288*, 112624. [CrossRef]
34. Zona, R.; Esposito, L.; Palladino, S.; Totaro, E.; Minutolo, V. Semianalytical Lower-Bound Limit Analysis of Domes and Vaults. *Adv. Non-Destr. Diagn. Mason.* **2022**, *12*, 9155. [CrossRef]
35. Zona, R.; Minutolo, V. A Direct Finite Element Limit Analysis for Assessing the Structural Safety of Masonry Under Anisotropic Behavior. *Int. J. Numer. Methods Eng.* **2025**, *126*, e70221. [CrossRef]
36. Palladino, S.; Zona, R.; Minutolo, V. Ancient Projectile Identification Through Inverse Analysis: Case Studies from Pompeii. *Eng. Proc.* **2025**, *96*, 8. [CrossRef]

Disclaimer/Publisher's Note: The statements, opinions and data contained in all publications are solely those of the individual author(s) and contributor(s) and not of MDPI and/or the editor(s). MDPI and/or the editor(s) disclaim responsibility for any injury to people or property resulting from any ideas, methods, instructions or products referred to in the content.